UNIVERSIDAD DE INGENIERÍA Y TECNOLOGÍA

CARRERA DE INGENIERÍA MECÁNICA

FLEXIBLE TPU PNEUMATIC ACTUATOR SIMULATION

TESIS

Para optar el título profesional de Ingeniero Mecánico

AUTOR

Julio Cesar San Martin Lopez (ORCID: 0000-0002-3025-8884)

ASESOR(ES)

José Garcia Bravo (ORCID: 0000-0002-3017-3354)

Brittany Newell (ORCID: 0000-0001-5737-2065)

Julien Noel (ORCID: 0000-0001-9284-9025)

Lima – Perú

2022

Dedico de manera especial a mis padres, por todo el sacrificio, esfuerzo y apoyo que han realizado para darme una educación de calidad. A las universidades UTEC y Purdue por brindarme oportunidades, experiencias y retos en el crecimiento de mi vida profesional. Finalmente, le dedico este trabajo a mi persona, para visualizar mi crecimiento a lo largo de mi época de educación y en lo que va en mi periodo profesional.

TABLE OF CONTENTS

TABLE INDEX

FIGURE INDEX

ANNEX INDEX

RESUMEN

Actuators are devices that provides a controlled change in a physical system. They can operate manually, electrically, or by various fluids. Among them, pneumatics actuators have advantages of working with compressible fluids that provides safety and efficient limitations. These are very critical parameters for soft robotics.

Rigid actuators are not suitable to substitute muscle functions, hence flexible actuators are appealing. Yet the process to fabricate soft actuators have long iteration until the final product is manufactured and is difficult to design and control due to their natural flexible behavior. 3D printing could be a possible solution. Researchers are exploring feasible solutions with 3D printing material. However, since it's a new area of research, there is not a large and deep characterization of these materials.

This study will focus on the simulation of a hyperelastic TPU model based on experimental data. Simulations were done utilizing the software ANSYS to characterize the behavior on mentioned model for a soft actuator usage. The results were consistent when the printing orientation of actuators was parallel (0°) to the strain direction of the actuators. Results were less consistent when utilizing a printing orientation of 45° or higher.

KEY WORDS:

3D printing; Thermoplastic polyurethane; Model validation, Soft actuator

ABSTRACT

FLEXIBLE TPU PNEUMATIC ACTUATOR SIMULATION

This report presents an Hyperelastic 5 Parameters Mooney-Rivlin model of a 3D Printed Segmented Flexible Pneumatic Actuator based on experimental data, with a ± 5% deviation error. The proposed report contains the mechanical results (Total Deformation and Equivalent von-Misses Stress) of the 3-D printed actuator utilizing thermoplastic polyurethane (TPU). Key elements for the respective simulation of the hyperelastic model behavior were the number steps applied, the applied boundary conditions, mesh size, computational cost, and characterization of mechanical properties based on the angle of 3D-printing orientation. By comparing with experimental data, the simulated model's behavior was validated.

KEYWORDS:

3D printing; Thermoplastic polyurethane; Model validation, Soft actuators

INTRODUCTION

Actuators are mechanical or electro-mechanical devices that provide a controlled change in a machine or a physical system, either by generating force, motion, heat or flow [1]. Actuators can be operated manually, electrically, or by various fluids such as air or liquid. Depending on the type of use that the person desires, there are several actuation mechanisms. Figure 0.1. shows a magnitude comparison of different actuation mechanisms, which can help in the selection of an appropriate actuator.
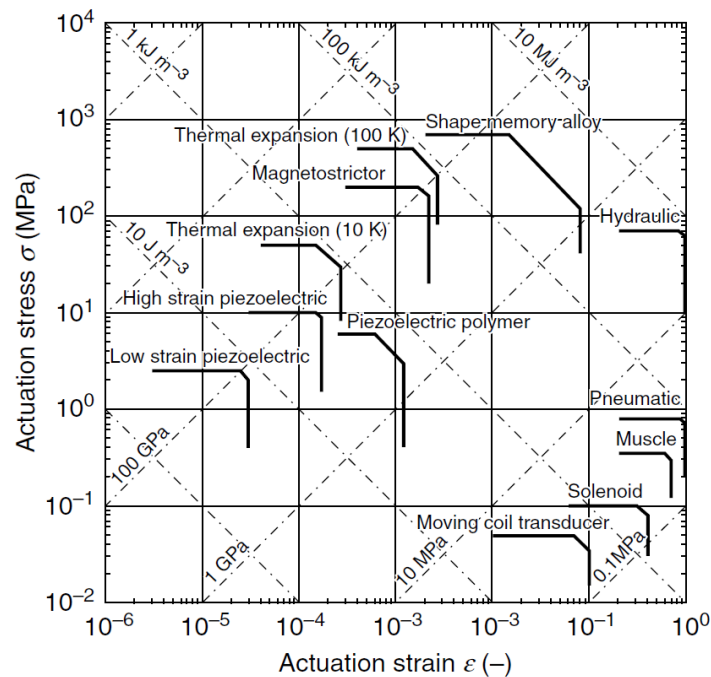
Figure 0.1. Actuation stress sigma versus actuation strain for various actuators [1].

Hydraulic and pneumatic actuators provide force and displacement via the flow of a pressurized fluid [2]. Pneumatic actuators have the advantage of working with more

compressible fluids, giving a boost to both safety and energy efficient limitations. Based on Figure 0.1., pneumatic actuators also give similar performance to muscle actuation devices, making it suitable to artificial substitute for muscle functions, such as with soft robotics. Soft robotics uses typically rely on the expansion and contraction of elastomeric chambers under positive or negative pressure, driven by pneumatic or hydraulic devices, known as Fluidic Elastomer Actuators (FEA) [3].

Nevertheless, there are some cases where a rigid actuator is not suitable for this function. Flexible actuators could be the solution for this case. Flexible actuators exhibit large deformation under an external signal with advantages of light weight, softness and arbitrary shape [4]. Most existing flexible actuators are made using multistep low-yield process such as micro-molding, solid freeform fabrication, and mask lithography. However, these processes require the manual fabrication of devices, post processing, and a lengthy iteration process until the final product is manufactured [5]. Researchers are exploring new ways to manufacture this type of actuators. 3D printing might be a feasible solution to manufacture faster and less expensive flexible actuators, also called 3D printed actuators.

This study will focus on the simulation of a hyperelastic TPU model based on experimental data. Simulations were done utilizing the software ANSYS to characterize the behavior on mentioned model for soft actuator usage.

1   CHAPTER I
LITERATURE REVIEW

This chapter presents a literature review of the materials used for soft actuators and the desire characteristics in order to select a material. Main hyperelastic models to simulate utilizing finite element analysis are also discussed.

1.1   Materials used for soft actuators

Hyperelastic materials are attractive for their ability to experience large deformation under small loads and to retain their initial configuration without a considerable permanent deformation after the load is removed. Their stress-strain curve presents a non-linear behavior and the properties for solid materials (Young's modulus, Poisson's ratio) are not sufficient to conduct a realistic simulation. The Young's modulus can be obtained with stress-strain tests and since there is little volume change in a hyperelastic material, they are considered incompressible, which is the equivalent of setting a Poisson's ratio of 0.499 [6].

A characterization of elastic behavior of nonlinear material is important to get an accurate behavior in the simulation. The material testing can be done with uniaxial, biaxial, planar shear, and volumetric tests [7]. The test data should represent the material that was created with the desired manufacturing processes.

Soft actuators materials need to be inspired by natural muscle and have a high strain density. Some of the most common materials are silicones and polyurethanes elastomers.

Silicone elastomers, also called silicone rubbers, are a range of heat stable elastic silicone materials used for high-performance industries applications, including mold-making, automotive, electronic and household item manufacturing. They are also very easy and economical to customize. Silicones elastomers also presents with resistance to high and low temperatures, high dielectric strength, sterilizability, durability, low flammability and good overall mechanical properties [8]. However, they required a curing process in order to obtain

their desired properties and they do not have a great chemical compatibility compared with other elastomers.

Polyurethanes elastomers are a class of polyurethane material that has characteristics similar to rubber. They present high elasticity, abrasion resistance, tear strength, chemical resistance and wide temperature compatibility [9]. Polyurethanes have a special class for 3D printing filament material, called thermoplastic Polyurethane (TPU). By combining both low and high polarity segments, TPU delivers a better combination of elasticity, rigidity, and flexibility. TPU has been usually used to 3D print products that require to bend or flex during application, while also having a firmer build while printing [10].

1.2   Hyperelastic models

There are many hyperelastic models (Mooney-Rivlin, Neo-Hookean, Full Polynomial, Yeoh, etc.) to simulate hyperelastic materials using finite element analysis (FEA). Selecting the best material model plays a key role in obtaining a successful simulation. Selecting the correct model can be chosen by selecting the best curve fit over the range of previous stress-strain analysis. ANSYS has automated curve fitting capabilities that can be used to quickly test several different models and automatically determine the necessary model coefficients for the simulation. Mooney-Rivlin model is often the best solution approach since it is one of the most stable hyperelastic laws [6].

Mooney-Rivlin hyperelastic model will be used in this study, which determines the stress state in a hyperelastic material by taking the derivatives of the strain energy density with respect to the strain components [11]. The only assumptions of utilizing a Mooney-Rivlin model are that the material is considered to be isotropic and incompressible.
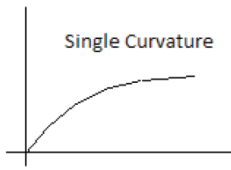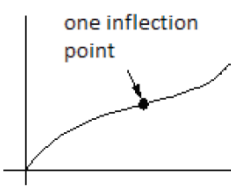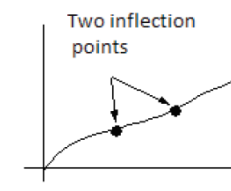
S.No.	Type of stress-strain curve	Type of Mooney-Rivlin model
1.	Single Curvature	2-parameters/3-parameters model
2.	one inflection point	3-parameters or 5-parameters model
3.	Two inflection points	5 –parameters or 9-parameters model

Figure 1.1. Types of Mooney Rivlin models [11].

In order to describe the material behavior, Mooney-Rivlin hyperelastic model uses a function of strain invariants with different parameters such as two, three, five or nine parameters model [11]. The selection of parameters depends on the type of the stress strain curve, as shown in Figure 1.1.

After the implementation of material properties and the selection of the proper hyperelastic model, testing of the material behavior is next. Test data should be compared with finite elements results for correct validation. Overcoming convergence issues can be solved with proper load control, adjusting the volume compatibility constraints and having a refined mesh.

2 CHAPTER II
EXPERIMENTAL SETUP AND SETTING

2.1 3d Printed Flexible Bellows Actuator

In order to start simulating utilizing TPU, a prior simulation needs to be made to validate the model that will be used. A model of a hollow bellow actuator was used to simulate. Figure 2.1. shows the model described.
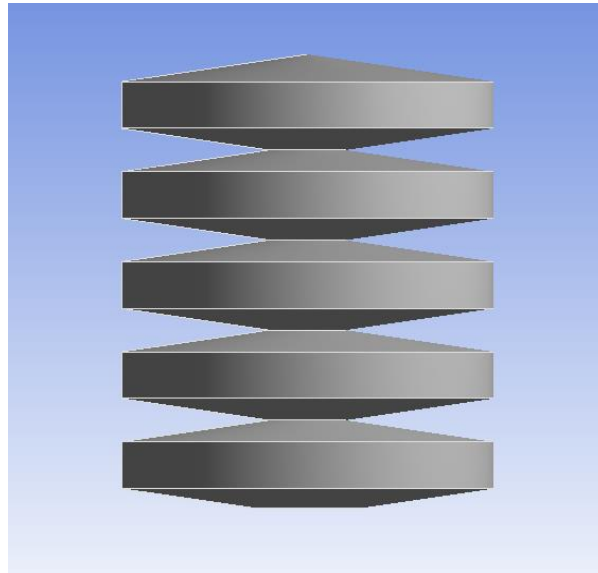
Figure 2.1. 3D Printed Bellows model actuator.

2.1.1 Simulation with Tango

The model consists of a bellow actuator with a fixed support at the edge of the bottom hole, where air will flow. A static structural analysis utilizing the software ANSYS was conducted by adding a pressure normal to the upper and lower inner walls of the actuator, with a ramping pressure up to 5kPa for 4s. The simulations were ran utilizing 20 steps and turning on the option for large deflection on the Analysis Settings branch. This option

allows ANSYS to account for changes in the stiffness due to changes in the shape of the parts that are simulating. In other words, as the object is deflecting, the stiffness also changes. This is very useful for objects that tend to be subjected to large deformations. Additionally, the method of element size was utilized to create the mesh for the simulation, with a mesh size of 1mm.
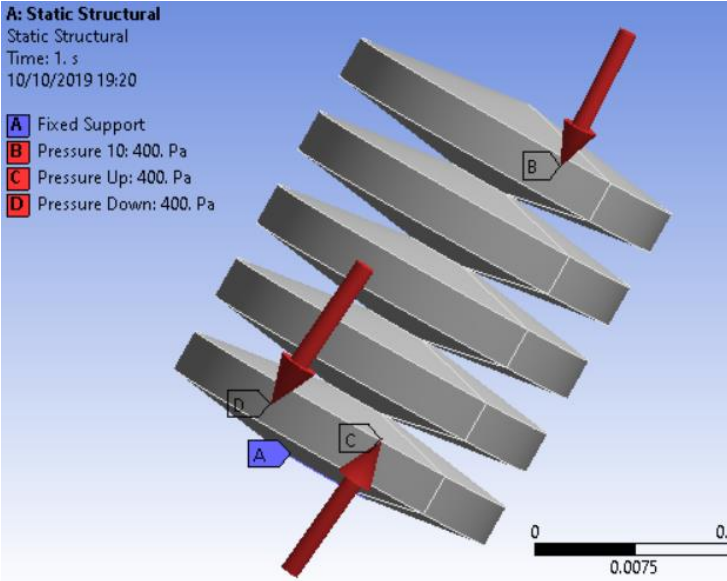
Figure 2.2. Boundary and initial conditions for the simulation model.

The properties of TangoPlus FLX930 were retrieved from the manufacturer manual [12] and Wohler's Report [13]. ANSYS is able to produce hyperelastic parameters if the stress-strain curve is provided. Table 2.1. provides the parameters needed to simulate a hyperelastic material utilizing Mooney-Rivlin 2 Parameter hyperelastic model.

Material Constant C10 (Pa)	Material Constant C01 (Pa)	Incompressibility Parameter D1 (Pa-1)
9.2563E+06	-4.7565E+06	0

Table 2.1. Coefficients of Mooney-Rivlin material model for Tango.

Mooney-Rivlin models express the mechanical strain energy as a sum of the invariants (functions of stretch ratios) with the following equation:

$$W = \sum_i . \sum_j C_{ij}(I_1 - 3)^i (I_2 - 3)^j + D(J - 1)^2$$

Where:

W: Strain Energy

C_{ij}: Coefficient

I_n; Invariants

J: Jacobian

D: Constant

Note that the constants C_{ij} and D are determined by curve-fitting measured stress-strain curves to the derivative of the equation [14]. If more parameters are utilized, the equation gets more complex, however, ANSYS facilitate this calculation and can interpret how stiff is the model based on the values of the coefficients.

The simulation was compared with a previous simulation done [15] in order to validate it.

2.1.2   Simulation with TPU

After the validation of the model, the material was changed to TPU. The same boundary and initial conditions were set. The properties for the TPU material were obtained via experimental data [16] and were categorized based on the numbers of layers (thickness) and the orientation of the printing orientation based on the direction of the applied external force. The printing angle was determined based on the width of each actuator. This means that with a 90° printing orientation, the filaments were perpendicular to the width of the

actuator, while with a 0 ° printing orientation, the filaments were parallel to the width of the actuator. Figure 2.3. shows three different printing orientation for the actuator.
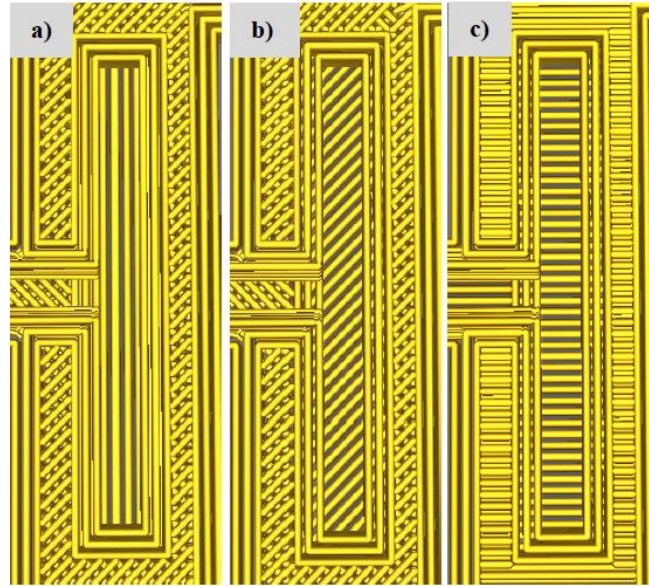
Figure 2.3. Printing paths for the actuation membrane at a) 90° ; b) 45° ; c) 0° [17].

Printing Orientation [°]	Maximum Stress [MPa]	Maximum Strain [mm/mm]
0	15.772	5.094
45	22.725	6.68
90	8.89	5.129

Table 2.2. Maximum stress and strain of experimental data.

Table 2.2. shows the maximum stress and strain experimental data. It seems that maximum stress and strain are achieved with a printing orientation of 45°, while the lowest strain and stress is achieved with a printing orientation 0° and 90° respectively.

Simulation was done for 0°, 45° and 90° and a one-layer (thickness: 0.2 mm) specimen. However, due to problems related with a high amount of iterations and

unconverged solutions in the simulations, it was decided to best work with only printing orientation of 0°. Comparison of the different effects to the mechanical results by changing the number of parameters within the model was the next objective of the following simulations. Table 2.3., Table 2.4., Table 2.5. and Table 2.6. provides the parameters obtained and needed to simulate TPU with 0° printing orientation as a hyperelastic material utilizing Mooney-Rivlin hyperelastic model with 2, 3, 5 and 9 parameters.

Material Constant C10 [Pa]	Material Constant C01 [Pa]	Incompressibility Parameter D1 [Pa-1]
6.7065E+05	2.6082E+06	0

Table 2.3. Coefficients of Mooney-Rivlin 2 parameter material model for TPU.

Material Constant C10 [Pa]	Material Constant C01 [Pa]	Material Constant C11 [Pa]	Incompressibility Parameter D1 [Pa-1]
-1.2561E+06	6.0846E+06	1.1151E+05	0

Table 2.4. Coefficients of Mooney-Rivlin 3 parameter material model for TPU.

Material Constant					Incompressibility Parameter D1 [Pa-1]
C10 [Pa]	C01 [Pa]	C20 [Pa]	C11 [Pa]	C02 [Pa]	
-2.7782E+07	3.86665E+07	87766	-7.5145E+05	9.2331E+06	0

Table 2.5.Coefficients of Mooney-Rivlin 5 parameter material model for TPU.

Material Constant					Incompressibility Parameter D1 [Pa-1]
C10 [Pa]	C01 [Pa]	C20 [Pa]	C11 [Pa]	C02 [Pa]	
-2.6927E+08	2.9813E+08	3.2555E+09	-7.0763E+09	4.0539E+09	0
C30 [Pa]	C21 [Pa]	C12 [Pa]	C03 [Pa]		
85956	-1.2753E+06	-8.0654E+08	5.2855E+0.8		

Table 2.6. Coefficients of Mooney-Rivlin 9 parameter material model for TPU.

Figure 2.4. shows the fitting for the Stress-Strain curve of the characterization of TPU material that ANSYS provides. It seems that utilizing 5 and 9 parameters Mooney-Rivlin models provides a better fit for the strain-stress curve of the TPU test data. As the number of parameters is increase, the fitted curve follows a more realistic behavior with the experimental data. However, it is important to analyze if the extra simulation power is worth increasing the numbers of parameters for the model.
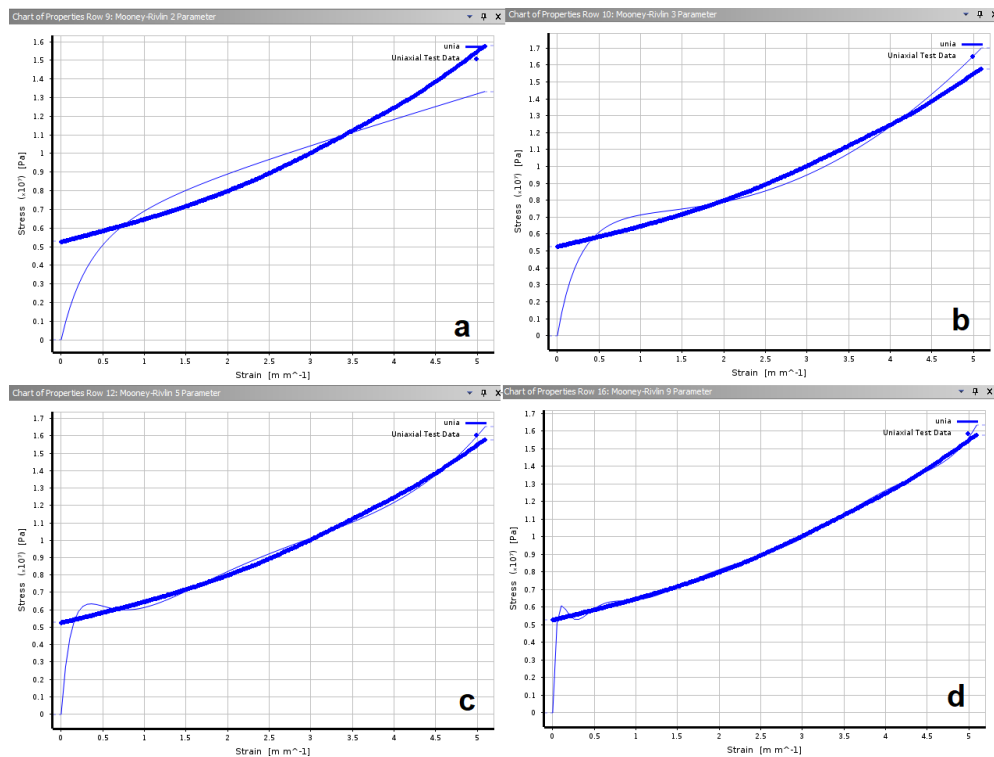
Figure 2.4. ANSYS's curve fit of experimental data with a) 2, b) 3, c) 5, d) 9 parameter Mooney-Rivlin.

The first iteration of simulation was made with a ramping pressure up to 5 KPa for 20s. The other iterations were made with higher pressure in order to determine the highest pressure that the current model can handle before unconvergence problems occurs. After the maximum pressure was discovered, simulation with the other parameters of Mooney-Rivlin model were tested to observe the differences that each model provides. Finally, a new type constrain was added to increase the pressure that the model can handle before unconvergence problems occurred.

2.2   3D printed segmented flexible pneumatic actuator

The second part of this study consists of comparing a previous experiment [17] of a 3D printed soft pneumatic actuator with a static structural simulation on ANSYS. Figure 2.5. shows the 3D printed model for the designed soft pneumatic actuator.
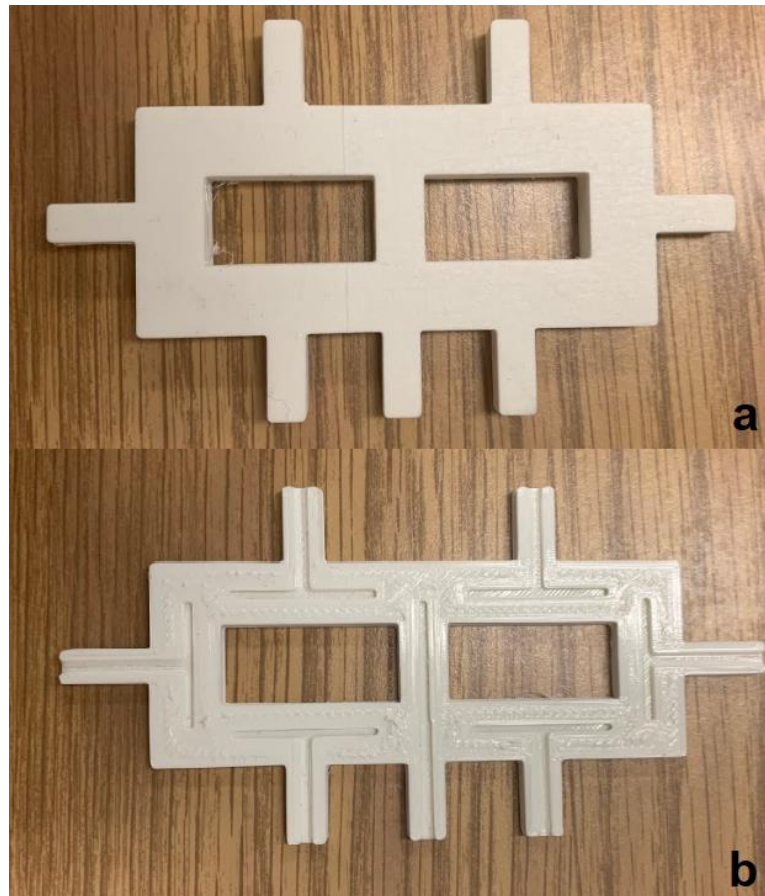
Figure 2.5. a) Complete 3D Printed segmented actuator model b) 3D Printed segmented actuator model with visible chambers.

The actuator consists of a seven-segment channels, with independent air inputs for each channel. Each input channel has a diameter of 2mm, providing the sufficient tightness to fully sealed the actuator to prevent air leakage.

The structure is made of three regions. The first region is a single layer with a thickness of 0.2mm, which is also called as membrane and is where the highest deformation

is expected to occur. The second region consists of a multi-layer zone with a thickness of 4mm. The third region is made of a multi-layer zone with a thickness of 2mm. These layers restrict the actuation in the negative z-direction, generating actuation only on the positive z-direction. Figure 2.6. shows the actuator composition with the different regions.
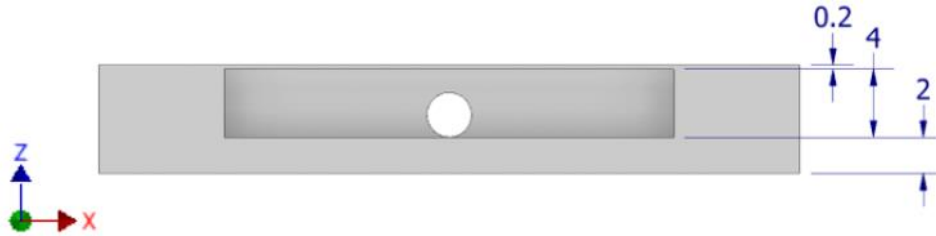
Figure 2.6. Actuator Composition [17].

The deformation is expected to have a behavior of a semi-ellipse, where the areas close to the edges present less deformation than the areas closer to the center of the membrane. Three different types of structures were printed, with printing orientations of 90°,45° and 0°.

The experiments characterized the displacement in z-axis based on the input pressure with a line of compressed air connected to a manual pressure regulator valve. The experiments were made by pressurizing only one channel and the analysis was based on the actuators with T-shape. Figure 2.7. shows the division to discretize measurement of displacement on the actuator.
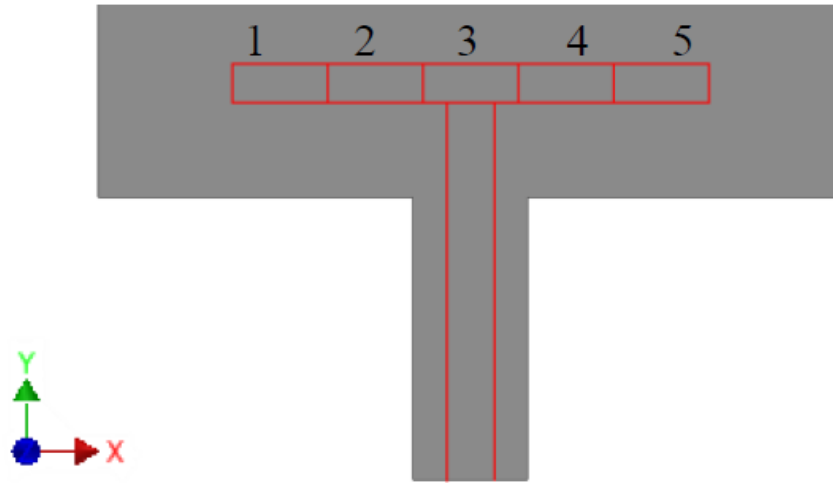
Figure 2.7. Division to discretize the pneumatic actuator and stablished the regions to measure the displacement [17].

For the purpose of this study, only the displacement on position 3 will be study. This is the position where the highest z-deformation occurs. The experimental displacements for each printing orientation and pressure input are shown in Table 2.7.

Pressure [kPa]	Displacement [mm] on Position 3		
	Printing Orientation 0°	Printing Orientation 45°	Printing Orientation 90°
70	0.06	0.09	0.15
103	0.09	0.15	0.25
138	0.11	0.20	0.28
172	0.14	0.26	0.35

Table 2.7. Displacement on position 3 of the pneumatic actuator [17].

The highest displacement result will be compared with the experimental results on Table 2.7. Several iterations changing the numbers of Mooney-Rivlin parameters and increasing and decreasing the size of the mesh, as well as simplified model were used to

develop a model that correlates well with the experimental results. The selection and validation of the model will be done if the simulated model has a deviation equal or less than ±5% with the four different pressures applied.

3   CHAPTER III

RESULTS AND DISCUSSION

3.1   3D printed flexible bellows actuator

3.1.1   Tango

Figure 3.1. shows the results of the simulation with TangoPlus FLX 930.
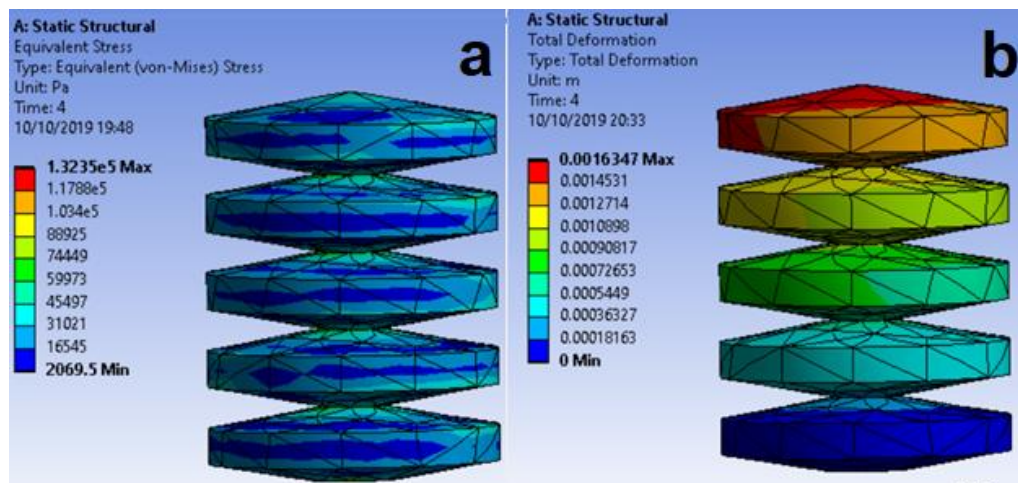
Figure 3.1. a) FEA stress analysis b) FEA deformation analysis for TangoPlus FLX 930.

A maximum deformation of 1.635 mm and a stress of 0.132MPa was obtained from the simulation. Based on the results of Figure 3.1.a, the behavior of distribution of the stress is very similar with the compared paper [15], with similar peaks of stress. The magnitude of the stress was very similar too. This validates the model for the use of the TPU analysis. However, the deformation was not the same. One of the solutions might be to implement the correct test data, since the test data for this simulation was acquired with the use of properties of the manufacturer and the properties might had change by the manufacturing process applied or the material itself.

3.1.2   TPU

Figures 3.2. and Figure 3.3. shows the deformation and stress results for the first iteration of simulations using TPU with a pressure of 5kPa.
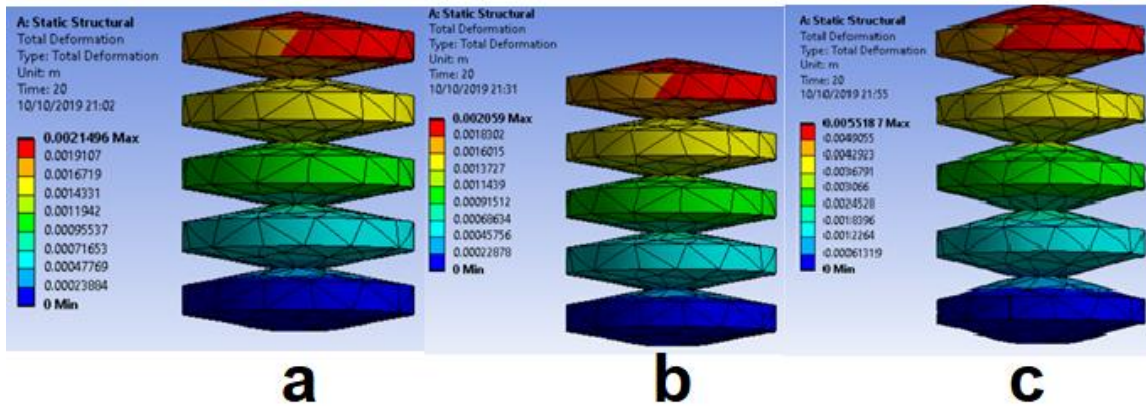
Figure 3.2. FEA deformation analysis with a) 0° b) 45°c) 90°for TPU.
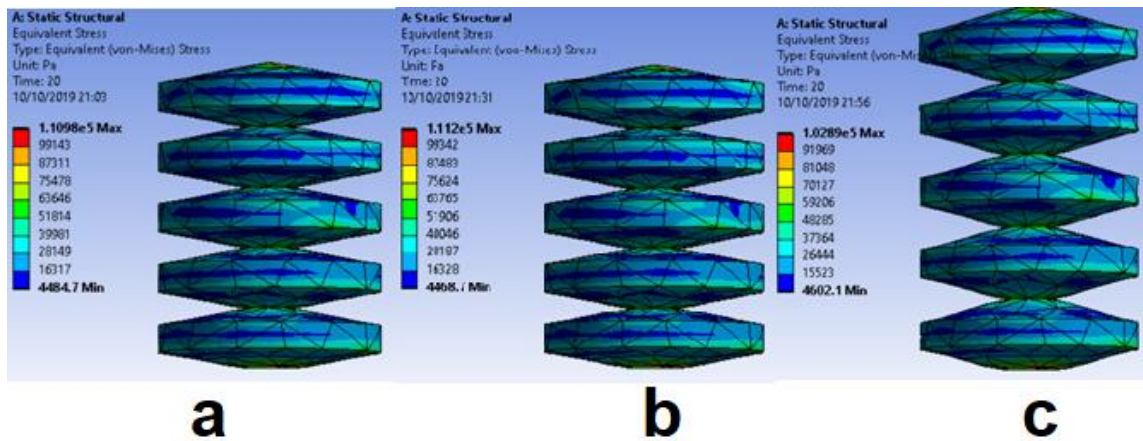
Figure 3.3. FEA stress analysis with a) 0° b)45° c) 90° for TPU.

Maximum deformations for 0°, 45°, and 90° were 2.149 mm, 2.059 mm and 5.519 mm respectively. Maximum stresses were 0.111 MPa, 0.111 MPa and 0.103 MPa respectively.

Deformation and stress results were very similar between 0° and 45°. 90° had larger deformation (more than double than 0° and 45°) and it had less stress that the others printing angles. TPU had better deformation and less stress when compared to Tango with the same pressure applied.

Figure 3.4. shows deformation and stress results of the second iteration with 138kPa of pressure applied.
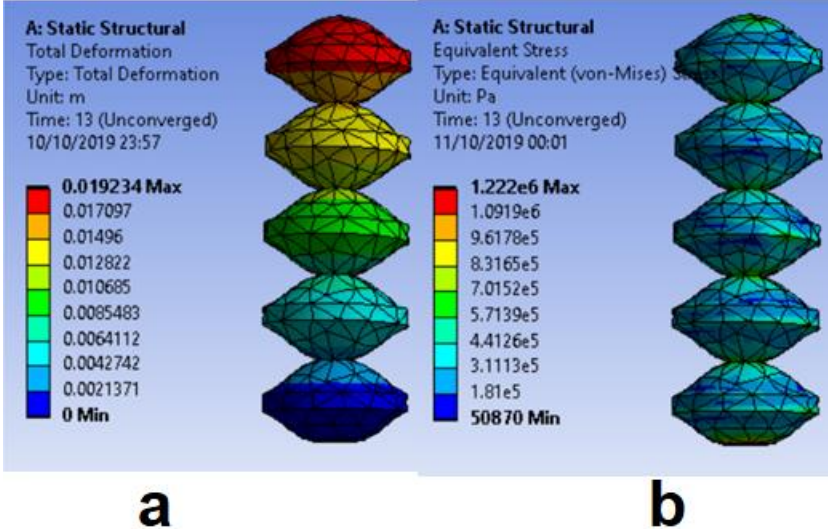
Figure 3.4. a) FEA deformation analysis b) FEA stress analysis for TPU 0°. Voltage vs. time graph example.

There was a convergence problem in the simulation, resulting in an error around 13 s. These results are not trustworthy, but it gives us an understanding of the behavior of the model subject to higher forces. Even with an applied pressure of 90kPa, the model still gave unconverged results. The maximum pressure that the current model could simulate without having unconverged problems was with 50kPa.

With this pressure, simulation with the different Mooney-Rivlin's parameters were done to observe the behavior of stress and strain on the model, as well as the processing time it takes to run the simulation.

Table 3.1. shows the results of stress and strain for each type of Mooney-Rivlin model.

Hyper Elastic Model	Stress [MPa]	Strain [mm]	Time [min]
Mooney-Rivlin 2 Parameter	2.07	14.5	65
Mooney-Rivlin 3 Parameter	2.26	11.15	60
Mooney-Rivlin 5 Parameter	2.59	5.95	54
Mooney-Rivlin 9 Parameter	2.82	2.51	45

Table 3.1. Results of Stress and Strain for each Mooney-Rivlin model.

Based on Table 3.1., it seems that as a more parameters are used in the model, the stress increases slightly. However, changing the type of parameter affects drastically the strain of the model, with the deformation utilizing a 9-parameter model being six times lower than utilizing a model with 2-parameters. Figure 3.5. facilitate the visualization of this behavior.
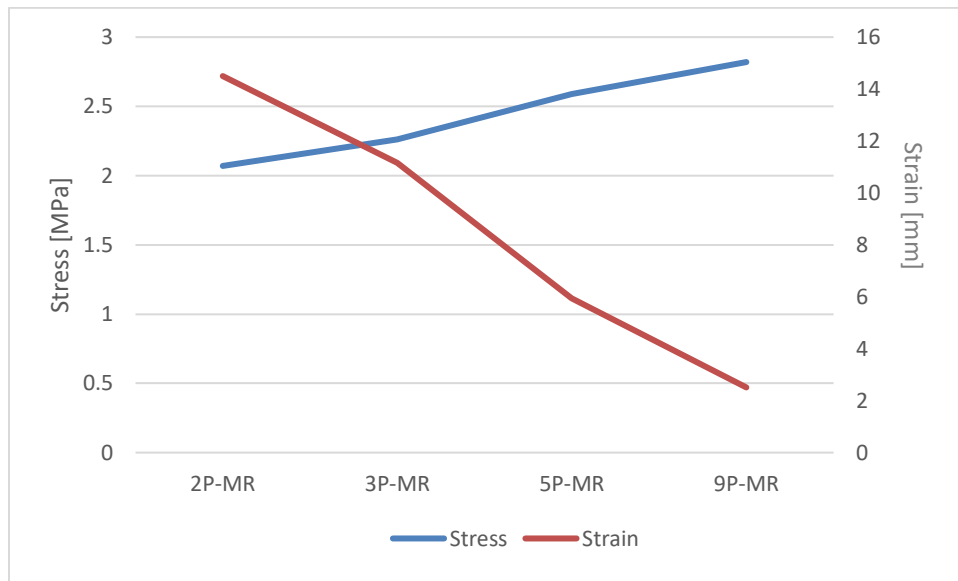
Figure 3.5. Stress and Strain vs number of parameter curve.

Additionally, it seems that the more precise model, the running time of the simulation decreases also. These results confirm that the selection of different hyperelastic models can changed drastically the mechanical results as well as the running time of the simulation.

To be able to simulate with higher pressure with the current model, an additional support was added to the faces of the model. Figure 3.6. shows the additional constrain added.
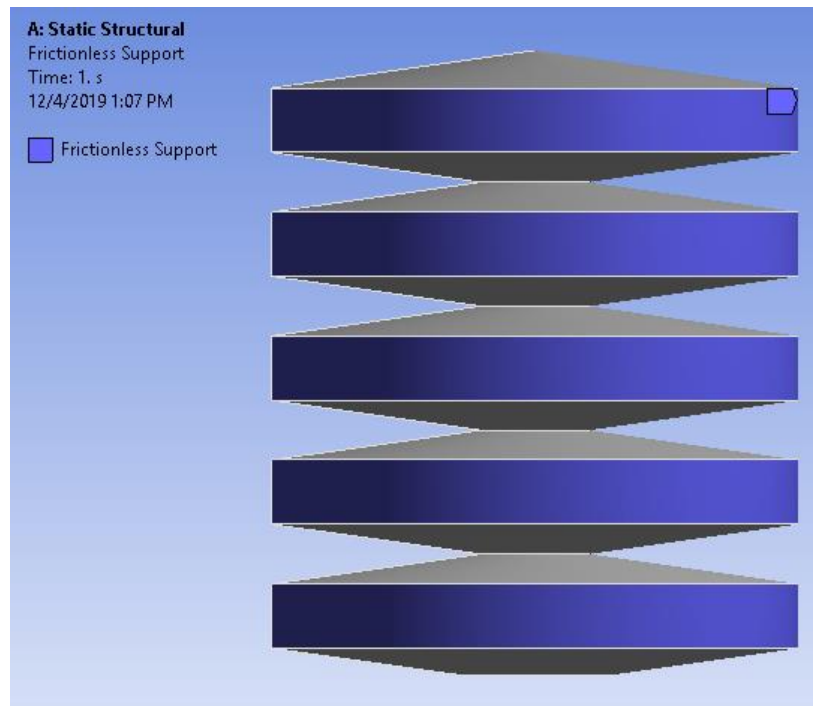
Figure 3.6. Additional frictionless support added to the model.

A frictionless support was added to alleviate the maximum pressure that model suffers at the fixed constrain at the edge of the model, since is in this area that the maximum stress occurs. A frictionless support applies constraints in the normal direction of the surface. This means that model was fixed of radial directions.

The pressure was able to reach up to 150kPa, three times the maximum pressure that the old model could handle. Table 3.2. shows the results of the simulations with the new constraint. All these simulations were ran utilizing a 5 parameter Mooney-Rivlin model.

Pressure [kPa]	Steps	Stress [MPa]	Strain [mm]	Time [min]
50	20	2.36	3.35	50
80	40	3.62	4.91	95
150	50	6.32	7.84	103

Table 3.2. Results of Stress and Strain with the new Bellows model.

A more reliable simulation can be done if the fixed support is changed from affecting the edge to affecting the surface of the bottom hole. This change could alleviate the stress that are generated in that zone, allowing to reach higher pressures.
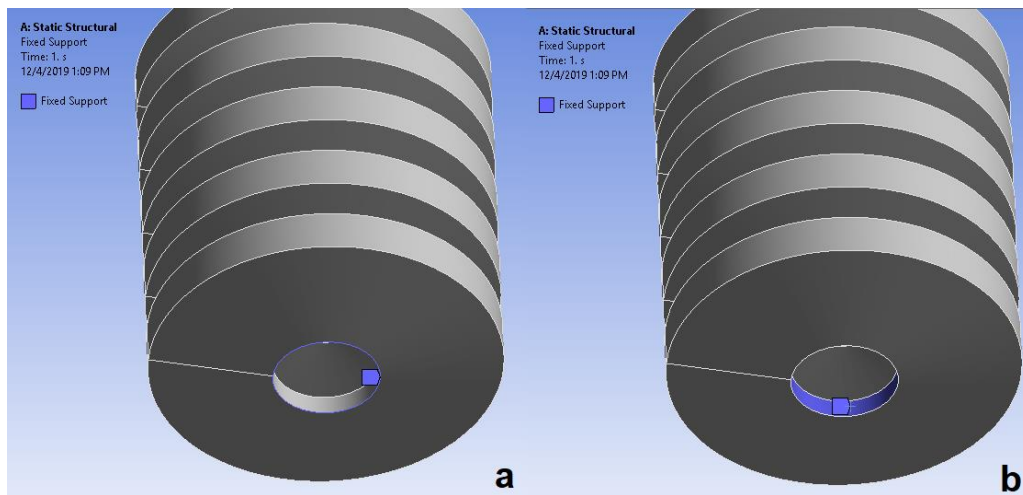
Figure 3.7. Change of placement of the fixed support on the model.

Nevertheless, these results were enough to get a better understanding of how to simulate the main flexible actuator of this study. This experiment concluded that the selection of the correct model is critical for the simulation, as well as the selection of the adequate initial conditions for the simulations.

3.2   3D printed flexible pneumatic actuator

3.2.1   Full model

The first set of iteration were done with the complete pneumatic actuator model. The first simulations were made to determine the hyperelastic model that best fit the experimental data for printing orientation of 0°. Mooney-Rivlin parameter 2,3, 5 and 9 were used for this purpose. Each simulation was analyzed with Structural Static ANSYS's module, simulating a stationary state with an increasing ramping pressure.

A fixed support was placed at the bottom of the third region of the actuator, with pressure on the inner walls and channels of the T-shape actuator, with 20 steps of applied pressure. The large deflections option was also turned on. The stress (VonMisses) and strain (Deformation) were analyzed for each pressure applied. An element size mesh option was utilized for the creation of the mesh, starting with an element size of 5mm up to 1.2mm. Further reduction of the area of the mesh resulted on unconvergence problems. Figure 3.8. shows the results of the simulations.

Figure 3.8. Comparison of utilizing different parameters models on a z-deformation versus element size curve.

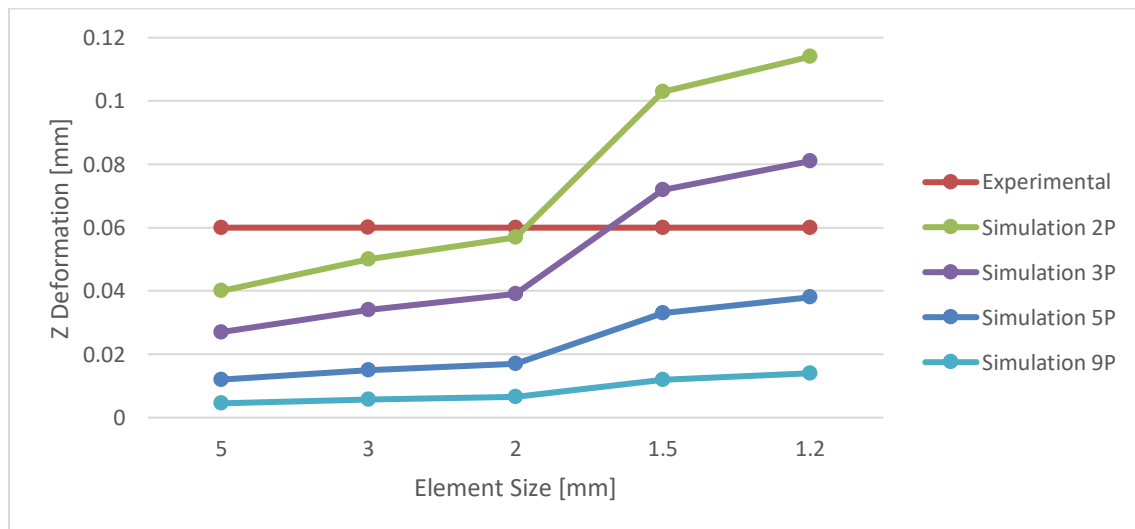Back on the previous figure, is possible to see a behavior that as the element size is reduce, the z-deformation increase. However, neither simulation was able to reach the z-deformation of the experiment until 1.5 mm element size was applied. With an element size of 1.5 mm, the model utilizing Mooney-Rivlin 2 parameters and 3 parameters experimented a z-deformation higher than the experimental data. As the element size was decreased to 1.2 mm, these models tend to drift away of the experimental data, while the models with 5 and 9 parameters were getting closer to the data. For this reason, Mooney-Rivlin with 5 parameters was chosen to be the model to use for further simulations. Table 3.3. shows the number of elements and nodes for each element size.

Element Size [mm]	Elements	Nodes
5	5694	10615
3	11178	20327
2	26943	46144
1.5	53529	87388
1.2	152877	96663

Table 3.3. Number of elements and nodes for each element size option.

However, a finer mesh is needed to obtain better z-deformation results, since Figure 3.8. showed that the finer the mesh, the model with 5 parameter Mooney-Rivlin tends to get closer to the deformation of the experimental data. A comparison of the 4 most relevant mesh size for the first set of experiment can be seen on Figure 3.9. The distribution of displacement also tends to align with the position of the inner channels as the elements size is reduce. This observation also gives a good reason to continue to decrease the element size of the mesh.
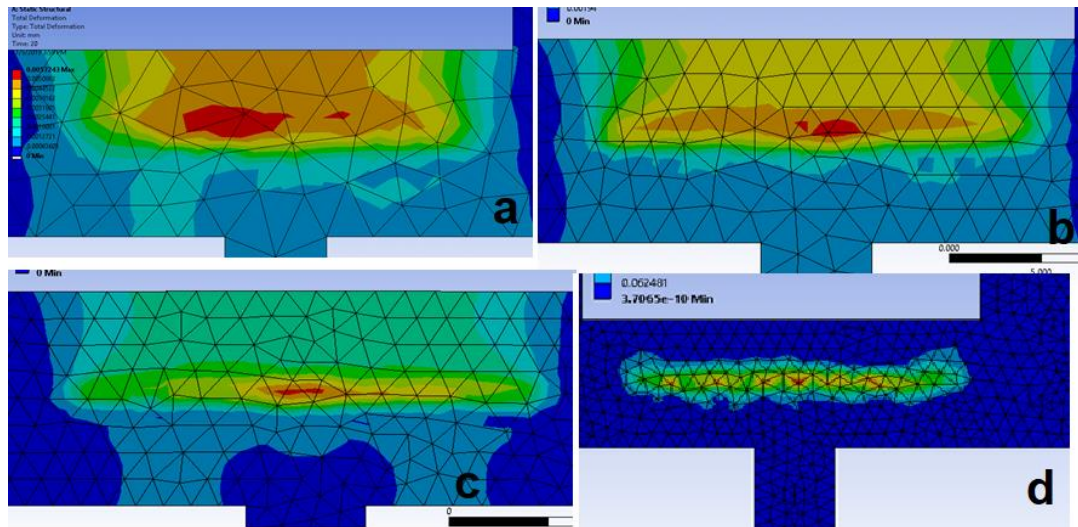
Figure 3.9. Visualization of the mesh and distribution of displacement utilizing element size of a) 3mm, b)2mm, c) 1.5mm, d) 1.2mm.

In order to get a finer mesh, it was decided to apply two meshing element size operations. The first element size would be applied to the walls and the lower surface of the actuator, while second element size would be applied only to the upper surface of the actuator, where the positive z-deformation will occur. The first simulations were done with an automatic mesh to the first element size operation, but they did not produce good results. The subsequent simulations were done with element size operation of 2mm and 1mm to the walls and the lower surface, while a 1mm and a 0.5 mm were applied to the upper surface. This produced a similar behavior with the results on Figure 3.9., while also increasing the number of elements to surface of analysis. Figure 3.10. shows the two types of meshing applied.
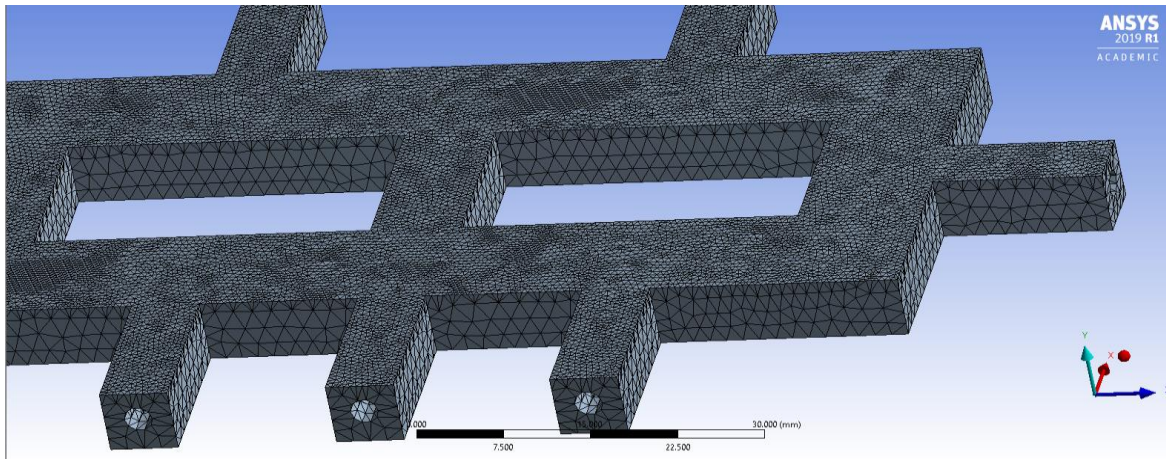
Figure 3.10. Visualization of the two types of meshing operations on the model.

However, even with this finest mesh applied, with 99208 number of elements, the displacement results were not close enough with the experimental data. The minimum error was 11%, not acceptable for the proposed 5% deviation error. Table 3.4. shows the mechanical results with an element size of 1.5 mm applied to the walls and the bottom for the actuator and with an element size of 0.58mm applied to the upper section of the actuator.

Pressure [kPa]	Mesh size [mm]	Stress [MPa]	Strain [mm]	Time [min]	Error [%]
70	0.6	0.957	0.0537	31	11
70	0.58	0.911	0.0534	31	11
103	0.6	1.361	0.0747	32	17

Table 3.4. Mechanical results of stress and strain with two types of mesh operations.

3.2.2 T-shaped model

It was decided to only simulate the T-shape section of the actuator, since the experiment was conducted with a single chamber. This also allows us to improve the mesh of the model. Since more elements could be put on the upper section of the model, a finer mesh could be created that will give better results. Figure 3.11. shows the T-shaped model.

Figure 3.11. T-Shaped model.

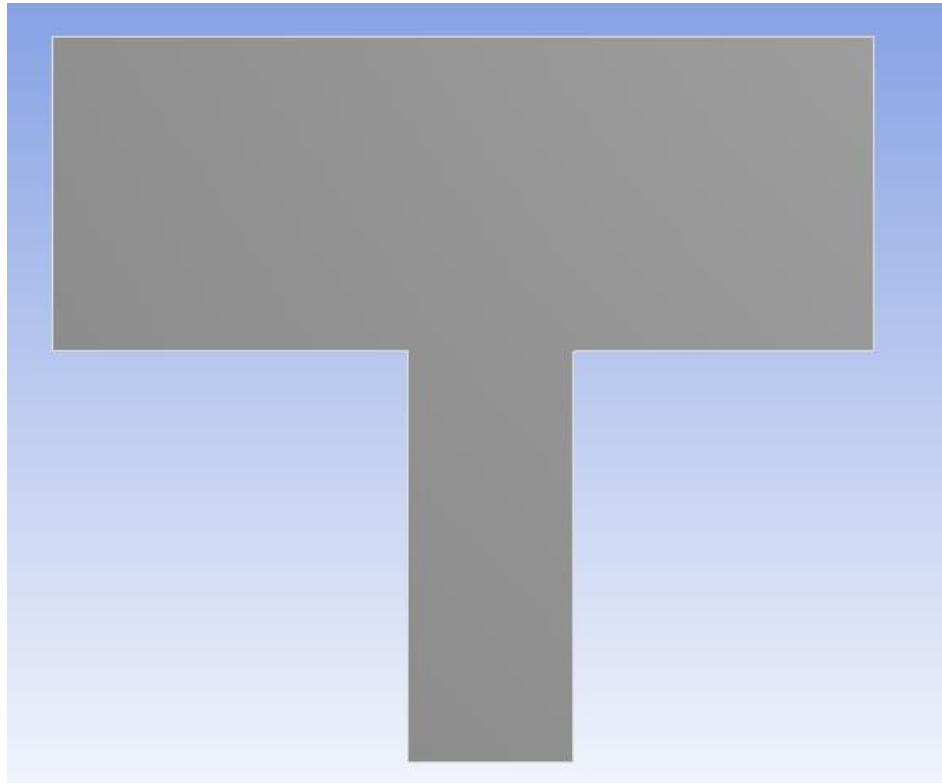1.5mm element size operation was used for the walls and the lower surface of the model, while element sizes of 0.5, 0.4, 0.3 and 0.2mm were tested. The results of the simulation can be seen on Table 3.5., as well as the comparison with the experimental strain for each pressure.

Pressure [kPa]	Mesh [mm]	Stress [MPa]	Strain [mm]	Exp. Strain [mm]
70	0.5	1.120	0.0611	0.06
70	0.4	1.096	0.0589	0.06
70	0.3	1.020	0.0596	0.06
70	0.2	1.359	0.0614	0.06
103	0.5	1.572	0.0845	0.09
103	0.4	1.536	0.0815	0.09
103	0.3	1.757	0.09	0.09
103	0.2	1.91	0.088	0.09
138	0.5	2.014	0.106	0.11
138	0.4	1.964	0.103	0.11
138	0.3	2.228	0.114	0.11
138	0.2	2.448	0.107	0.11
172	0.5	2.415	0.1257	0.14
172	0.4	2.3507	0.1215	0.14
172	0.3	2.649	0.1332	0.14
172	0.2	2.936	0.1262	0.14

Table 3.5. Comparison of mechanical results for T-Shaped model.

The stress results seems to follow a behavior similar to a convex as the mesh size reduces, while the strain seems to be stable, with little overall variation. An error-deviation analysis was made to determine the best element size for the model. Figure 3.12. shows the error for each element size z-deformation results versus the experimental z-deformation data.
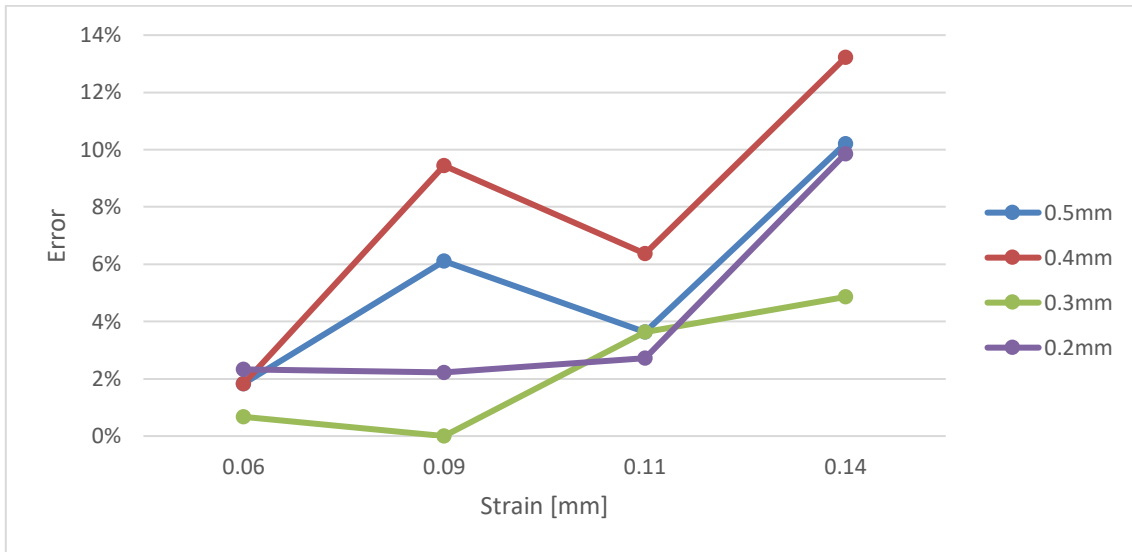
Figure 3.12. Error-deviation analysis curve.

The model that best behave the experimental data is with 0.3mm element size, with a total of 45419 elements. The maximum deviation with the experimental data was 5% at 138kPa pressure, however it had 1%, 0% and 4% error with pressures of 70kPa, 103 kPa and 138kPa respectively. Figure 3.13 shows the distribution of the total deformation with element size of 0.3mm.

Figure 3.13. Distribution of total deformation with element size 0.3mm.

With fulfilling the 5% error-deviation margin proposed, a 5 parameter Mooney-Rivlin, with an element size operation of 1.5mm for the walls and the lower surface, 0.3m element size for the upper surface and 20 steps is the selected model that best fit the experimental for the printing direction of 0°. Figure 3.14. shows the z-deformation behavior of the experiment and the model chosen.
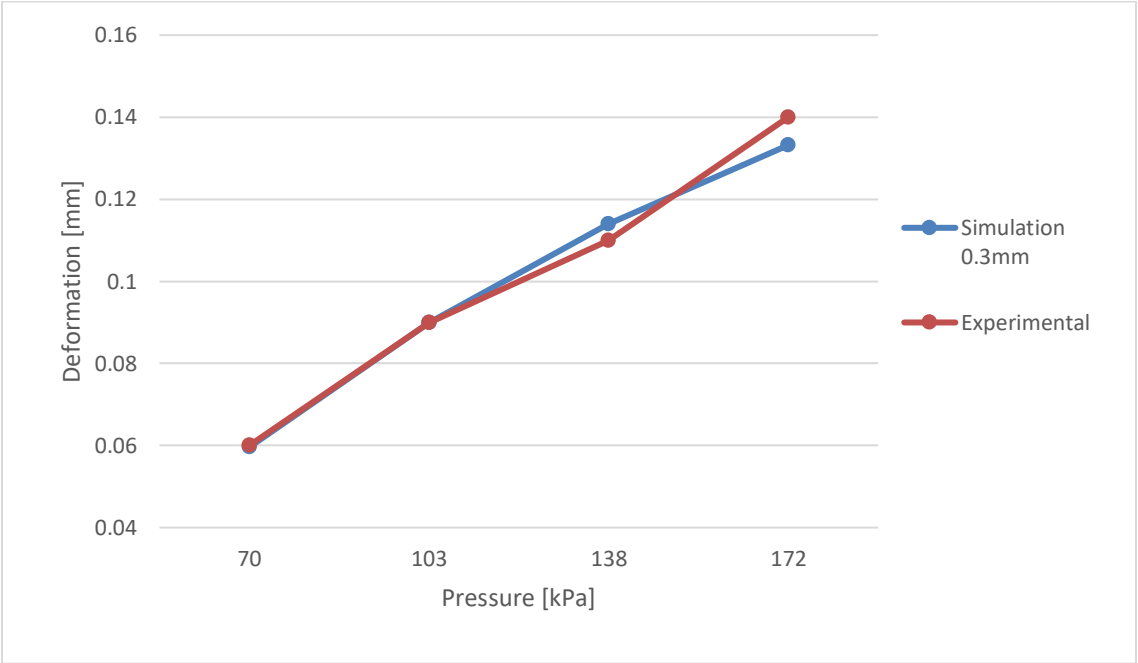
Figure 3.14. Z-deformation of simulation vs z-deformation of the experiment curve.

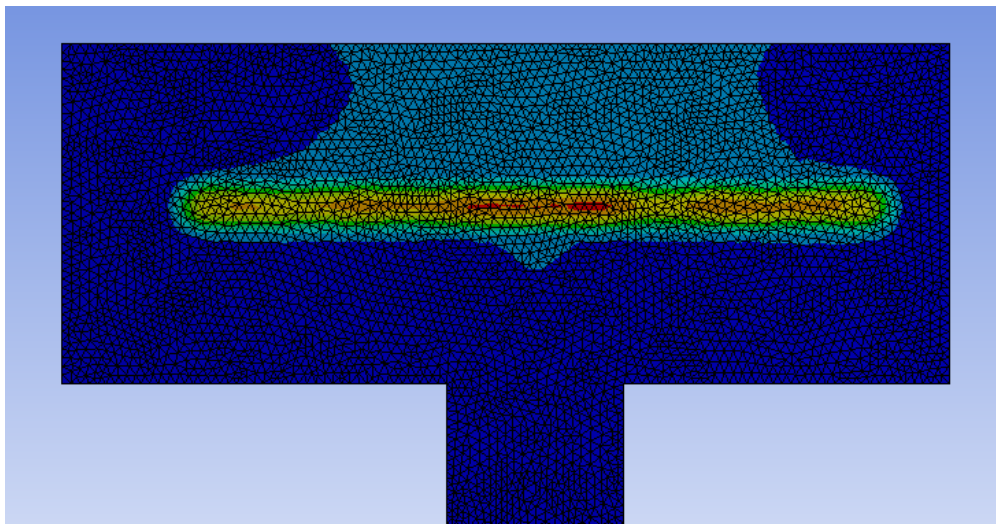The results of the previous figure show a good fit with model for the experiment, with an almost identical z-deformation.

To further validate the model, a convergence study was made. Mesh convergence tells us the lowest amount of elements required in a model to ensure that the results of an analysis are not affected by changing the size of the mesh [17]. This technique allows us to allocate the sufficient simulation power to obtain trust-worthy results, reducing the time it takes to simulate while also guaranteeing a tolerance zone for future simulations. Figure 3.15. and Figure 3.18. shows the convergence curve for strain and stress against the level of mesh refinement (number of elements).
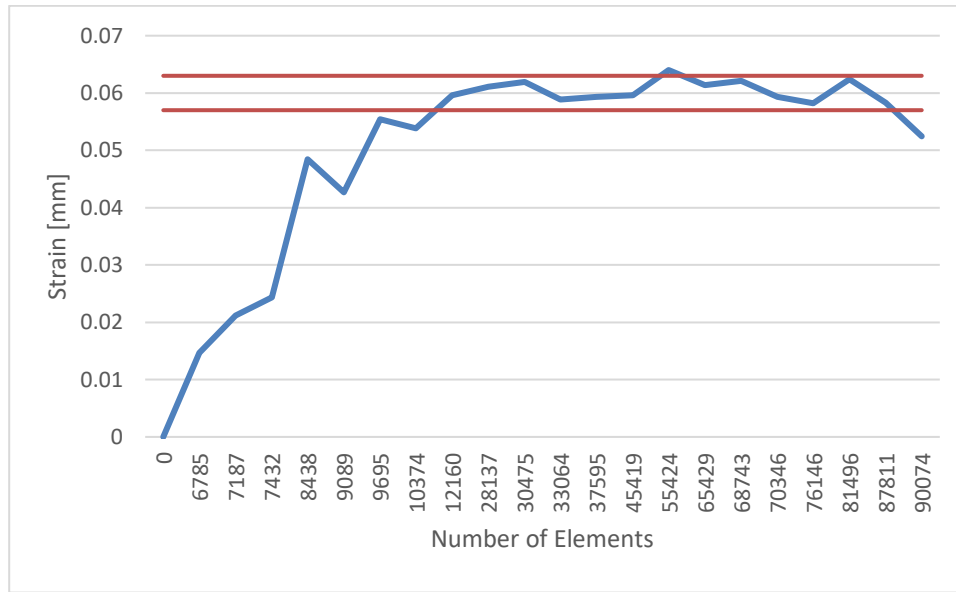
Figure 3.15. Strain convergence curve for the proposed model.

Figure 3.15. shows the effect of the maximum displacement while increasing the number of elements on the mesh. The two orange lines on the graph represent the ±5% proposed error-deviation. The minimum number of elements required for the model is 12,000 approximately, while the maximum number of elements required is 88,000 approximately. This gives us a tolerance zone of 12,000-88,000 number of elements required for the mesh, or 0.6-0.175mm on element size. The model also seems to fall of the 5% error-deviation standard when utilizing more than 90,000 number of elements, with an unreliable error of 13%.
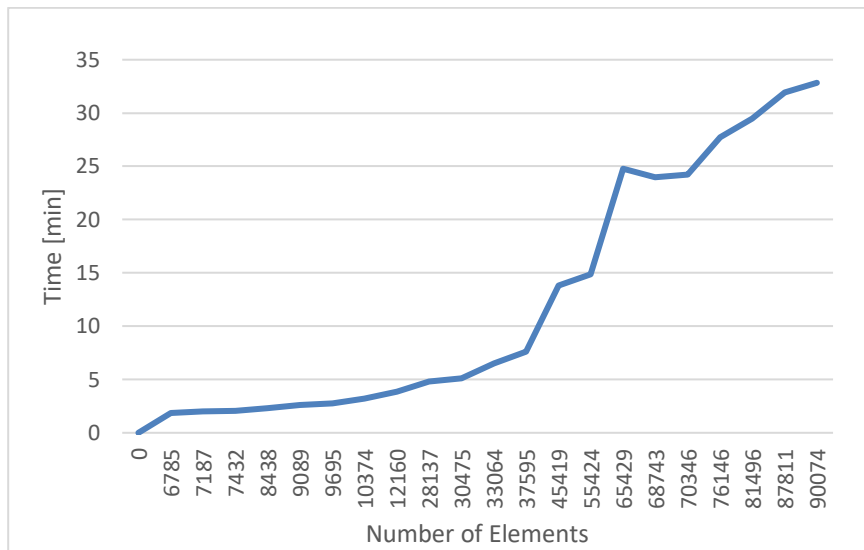
Figure 3.16. Time it takes to run the simulation vs the number of elements on the simulation.

Figure 3.16. reflects the processing time with the number of elements. There seems to be a peak of time increase when the number of elements is higher than 40,000. With the proposed tolerance for the element seize, the simulation takes 3 minutes with the minimum number of elements, while it takes 32 minutes with the maximum number of elements. Figure 3.17. shows the results utilizing the minimum required number of elements.
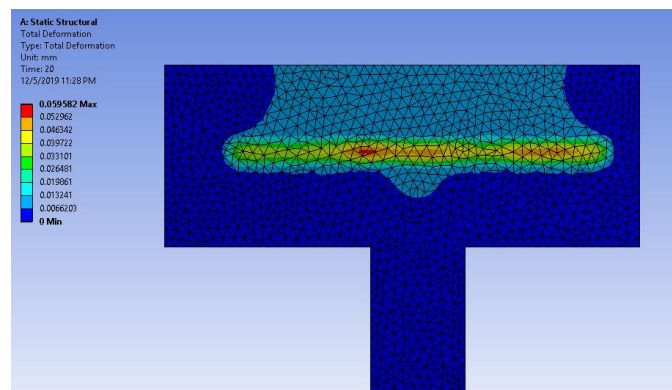
Figure 3.17. Total Deformation results with element size of 0.6mm.

Thanks to the convergence study, 29 minutes of processing time can be saved if the lowest allowable number of elements is used, with only 1% of error-deviation with respect of the experimental data.
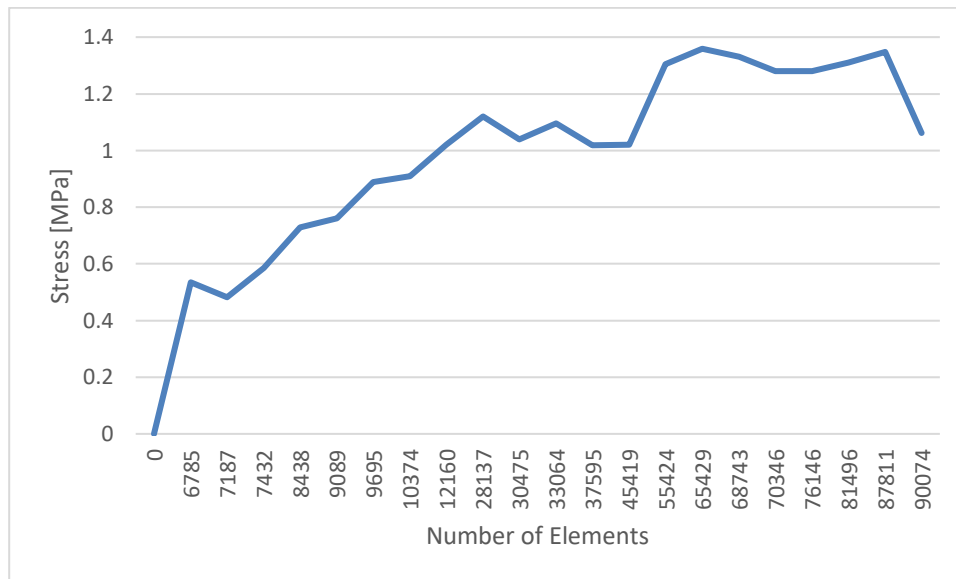
Figure 3.18. Stress convergence curve for the proposed model.

Regarding stress, the stress convergence curve shows that results are not as stable as the deformation. It seems that the stress is stable at 1.03 MPa within 12,000 to 45,000 number of elements. Then, the stress is increased up to 1.3MPa from 55,000 to 87,000 number of elements. Finally, like the strain curve, the stress tends to fall down drastically when utilizing more than 90,000 number of elements.

One key parameter that was never changed during the simulations was the number of steps applied. A simulation with 100 steps, instead of the 20 steps applied, was conducted and had favorable resulting regarding deformation and stress.
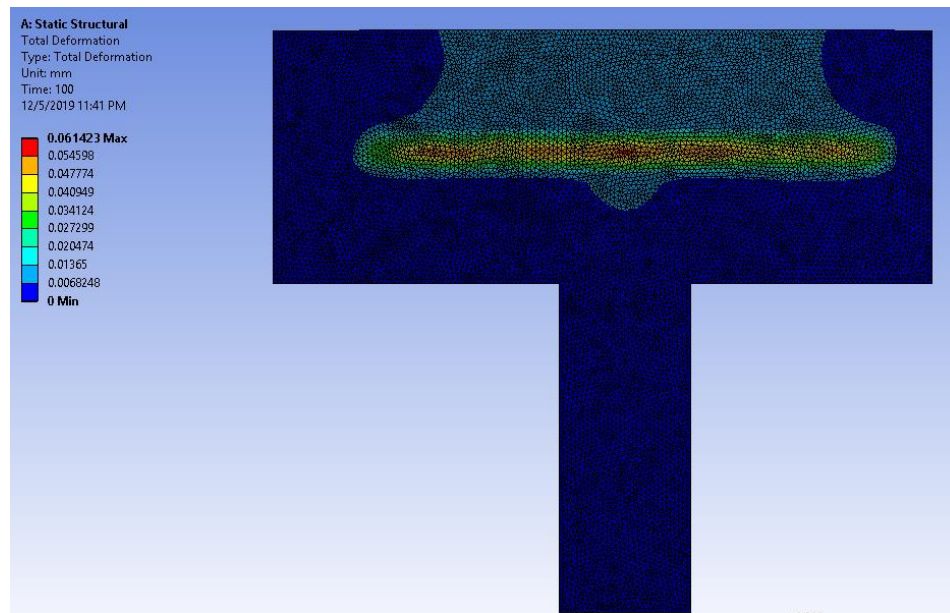
Figure 3.19.Total Deformation results for simulation with 100 steps.

The total deformation was 0.0614mm, with an error-deviation of 2%. However, this simulation took 2 hours to complete, more than four times the duration it took with the finest mesh. For this reason, it is not recommended to work with more than 20 steps, since even if it provides with good mechanical results, the cost of operating time is too high for it to be beneficial in future studies.

3.2.3 Proposed hyperelastic model

The proposed hyperelastic 3D printed Segmented Flexible Pneumatic actuator utilizing TPU with a printing orientation of 0° is the following.:

- Model: 5 Parameter Mooney-Rivlin

$$W_{(5)}=-2.778E^{+07}(I_1-1)+3.86665E^{+07}(I_2-1)+87766(I_1-1)^2$$
$$-9.23331E^{+06}(I_2-1)^2-7.5145E^{+05}(I_1-1)(I_2-1)+0(J-1)^2$$

- Number of required steps: 20 ramped steps
- Number of elements required: 12,000
- Processing time: 3 minutes (minimum)
- Error: 1%
- Constraints: 1 fixed support at the bottom of the actuator

The selected model was used to simulate with printing orientation of 45°. However, the results did not correlate well with the experimental data. The T-shaped model was changed to a 5 parameter Mooney-Rivlin, with a 0.8mm element size for the walls and the lower surface of the model and 20 steps. The model was tested with an element size mesh operation of 0.5mm and 0.2mm on the upper surface of the model. The results can be seen in Table 3.6.

PRESSURE [KPA]	MESH [MM]	STRESS [MPA]	STRAIN [MM]	TIME [MIN]	ERROR [%]
70	0.5	1.045	0.0659	20	27
70	0.2	1.336	0.0733	44	19
103	0.5	1.464	0.0904	21	40
103	0.2	1.828	0.0994	49	34
138	0.5	1.872	0.113	21	44
138	0.2	2.29	0.123	49	39
172	0.5	2.24	0.133	20	49
172	0.2	2.703	0.143	49	45

Table 3.6. Mechanical results for printing orientation of 45°.

The results do not correlate well with the experimental data, even with a finer mesh than the one used on the model with 0° printing orientation, the model for the 45° could not reach the experimental data. The finer model with 0.2mm element size was chosen as the best model for this 45° printing orientation. However, even with this model, errors of 19%, 34%, 39% and 45% occurred for pressures of 70kPa, 103kPa, 138kPa and 172kPa respectively. The z-deformation behavior for the experimental data and the model mentioned can be seen on Figure 3.20.
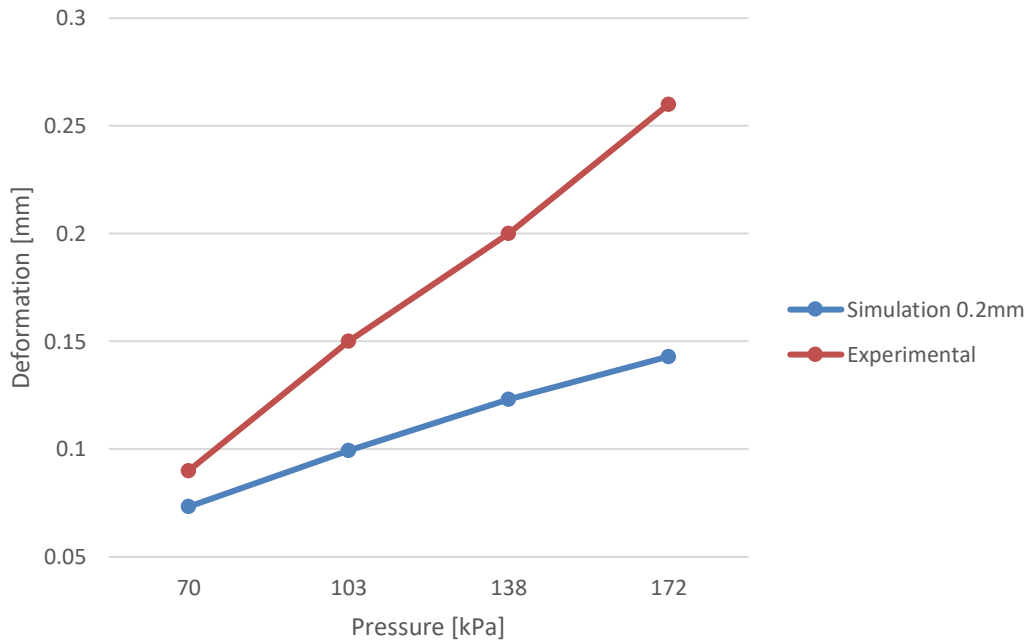
Figure 3.20 Z-deformation of simulation vs z-deformation for 45° of the experiment curve.

A comparison with the perfect fit with printing orientation of 0°, the model proposed does not fit with the experimental data. Simulation with printing orientation of 90° also provided no reliable outputs. This is because with printing orientation of 0°, the model behaves very similar to a solid element. By changing the printing orientation, the material starts to become anisotropic. While simulating with Static Structural module and utilizing a Mooney-Rivlin model, the software assumes an incompressible hyperelastic solid with isotropic properties. Further studies could be done with composite material or additive manufacturing models in order to get a better behavior utilizing printing orientation of 45° and 90°.

CONCLUSIONS

This study managed to build a Mooney-Rivlin hyperelastic model for a 3D printed segmented flexible pneumatic actuator made of TPU. The results obtained conclude that utilizing a 5-parameter model is the best fit in term of mechanical results as well as acceptable processing time, while applying certain assumptions (isotropic behavior, stationary state, etc.). The simulations also concluded that the selection of the appropriate number of steps, the suitable boundary conditions, the element size of the mesh and the hyperelastic model that best fit the Stress-strain curve, are all critical aspects to obtain a reliable result. Iterative simulations were done to provide mesh convergence that resulted in a tolerance zone for the number of elements required for the mesh. With good simulations practices, is possible to obtain a reliable simulation with low cost in term of computational power and time.

This model only correlates with a printing orientation parallel to the width of the actuator (0°). When using a printing orientation different from 0°, it is not possible to assume that the material can be treated as a solid element. For the analysis of different printing orientations, it would be convenient to utilize Composite or Additive Manufacturing modules to obtain more realistic behaviors, as well as more complex hyperelastic models.

Further steps should be to analyze different types of elastic printing filaments, with printing orientation of 0°. More complex soft actuators designs with TPU could be tested experimentally and via simulations, utilizing this model, to further collaborate the capability of the model. If the model proofs good correlations, this could facilitate the characterization of new printing filaments and could even help align the goals of researchers and engineers with 3D printing filament companies in order to obtain the desired properties needed for new generation of soft actuators.

BIBLIOGRAPHY

[1] P. K. Sekhar and V. Uwizeye, "2 – Reiview of sensor and acutator mechanisms for bioMEMs," *In Woodhead Publishing Series in Biomaterial,* pp. 46-77, Dec. 2012, doi: 10.1533/9780857096272.1.46

[2] J. E. Huber, N. Fleck, and M. Ashby, "The selection of mechanical actuators based on performance indices," *Proc. R. Soc. Lond. A.*, pp. 2185-2205, Oct. 1997, doi:10.1098/rspa.1997.0117

[3] A. Miriyev, G. Caires, and H. Lipson, "Functional properties of silicone / ethanol soft-actuator composites," *Materials & Design*, vol. 145, pp. 232–242, May 2018, doi: 10.1016/j.matdes.2018.02.057

[4] W. Chen and Z. Zhu, "Flexible Actuators", *Handbook of Smart Textiles*, pp. 381-410, Jan. 2015, doi: 10.1007/978-981-4451-45-1_20

[5] A. Zolfagharian et al., "Evolution of 3D printed soft actuators," *Sensors & Actuators: A. Physical*, vol. 250, pp. 258–272, Oct. 2016, doi: 10.1016/j.sna.2016.09.028

[6] P. Barret, "Tips & Tricks for FEA Modeling of Rubber and Elastomers," *CAEAI,* 2016. [Online]. Available: https://caeai.com/blog/tips-tricks-fea-modeling-rubber-and-elastomers-part-1

[7] M. Shahza et al., "Mechanical Characterization and FE Modelling of a Hyperelastic Material," *Material Research*, vol. *18*(5), pp. 918–924, Oct. 2015, doi: 10.1590/1516-1439.320414

[8] SIMTEC, "Pros and Cons of Silicone Elastomers." 2016. [Online]. Available: https://www.simtec-silicone.com/pros-cons-silicone-elastomers/

[9] Corrosionpedia, "Elastomeric Polyurethane," Nov. 2018. [Online]. Available: https://www.corrosionpedia.com/definition/4964/elastomeric-polyurethane

[10] J. Flynt, "The Properties of Flexible TPU Filament, How to Work with it, and Best Brands," *3dinsider*, Mar. 2018. [Online]. Available: https://3dinsider.com/tpu-filament/

[11] N. Kumar and V.V. Rao, "Hyperelastic Mooney-Rivlin Model : Determination and Physical Interpretation of Material Constants," *MIT International Journal of Mechanical Engineering*, vol: *6*(1), pp 43–46, 2016, ISNN: 2230-7680

[12] F. Tango, "Polyjet simulated rubber material," *Stratasys*, 2018.

[13] J. Mireles, "Appendix E : Material properties Stereolithography," *Wohlers Report*, pp. 1–59, 2011. [Online] Available: http://www.wohlersassociates.com/materials2011.pdf

[14] B. McGinty, "Mooney-Rivlin Models," *Continuum Mechanics*, 2012. [Online]. Available: https://www.continuummechanics.org/mooneyrivlin.html

[15] A. Costas, B. Newell, and J, Garcia. "Production and Characterization of a Fully 3D Printed Flexile Bellows Actuator," *Conference on Smart Materials, Adaptive Structures and Intelligent Systems*, pp. 1–8, Sep. 2019, doi: 10.1115/SMASIS2019-5644

[16] D. Gonzalez, J. Garcia, and B. Newell, "Sensors and Actuators A : Physical Electromechanical characterization of a 3D printed dielectric material for dielectric electroactive polymer actuators," *Sensors & Actuators: A. Physical*, vol: *297*, 111565, Oct. 2019, doi: 10.1016/j.sna.2019.111565

[17] D. Gonzalez, J. Garcia, and B. Newel, "3D PRINTED SEGMENTED FLEXIBLE PNEUMATIC ACTUATOR," *Smart Materials, Adaptive Structures and Intelligent Systems,* pp. 1–7, Dec. 2019, doi: 10.1115/SMASIS2019-5645

[18] NAFEMS, "The Importance of Mesh Convergence," 2019. [Online]. Available: https://www.nafems.org/join/directory/knowledge-base/the-importance-of-mesh-convergence-part-1/

[19] S. Torres, J. San Martin, B. Newell, and J. Garcia, "SIMULATION AND VALIDATION OF FULLY 3D PRINTED SOFT ACTUATORS," *Smart Materials, Adaptive Structures and Intelligent Systems, pp. 1-8, Nov 2020, doi:* 10.1115/SMASIS2020-2240

ANNEXES

ANNEX 1: ACTUATOR DIMENSIONS [19]

Dimension	Value
A	1.23 mm
B	3.24 mm
C	31.46 mm
D	26.53 mm
E	16.26°
F	1.50 mm